Robust zero-energy bound states around a pair-density-wave vortex core in locally noncentrosymmetric superconductors

Yoichi Higashi,[1,*] Yuki Nagai,[2] Tomohiro Yoshida,[3,†] Yusuke Masaki,[4] and Youichi Yanase[5,‡]

[1]*Department of Mathematical Sciences, Osaka Prefecture University, 1-1 Gakuen-cho, Naka-ku, Sakai 599-8531, Japan*

[2]*CCSE, Japan Atomic Energy Agency, 178-4-4, Wakashiba, Kashiwa, Chiba 277-0871, Japan*

[3]*Graduate School of Science and Technology, Niigata University, Niigata 950-2181, Japan*

[4]*Department of Physics, The University of Tokyo, Tokyo 113-0033, Japan*

[5]*Department of Physics, Niigata University, Niigata 950-2181, Japan*

(Received 25 February 2015; revised manuscript received 1 February 2016; published 29 March 2016)

We numerically investigate the electronic structures around a vortex core in a bilayer superconducting system, with s-wave pairing, Rashba spin-orbit coupling, and Zeeman magnetic field, with the use of the quasiclassical Green's function method. The BCS phase and the so-called pair-density-wave (PDW) phase appear in the temperature-magnetic-field phase diagram in a bulk uniform system [T. Yoshida *et al.*, Phys. Rev. B **86**, 134514 (2012)]. In the low magnetic field perpendicular to the layers, the zero-energy vortex bound states in the BCS phase are split by the Zeeman magnetic field. On the other hand, the PDW state appears in the high magnetic field, and the sign of the order parameter is opposite between the layers. We find that the vortex core suddenly shrinks and the zero-energy bound states appear by increasing the magnetic field through the BCS-PDW transition. We discuss the origin of the change in the vortex-core structure between the BCS and PDW states by clarifying the relation between the vortex bound states and the bulk energy spectra. In the high-magnetic-field region, the PDW state and vortex bound states are protected by the spin-orbit coupling. These characteristic behaviors in the PDW state can be observed by scanning tunneling microscopy/spectroscopy.

DOI: 10.1103/PhysRevB.93.104529

I. INTRODUCTION

Exploring the unconventional or exotic superconducting phase has attracted great interest and has been one of the streams of superconductivity research [1–3] since the Cooper pair wave functions have internal degrees of freedom reflecting the additional symmetry breaking other than the gauge symmetry $U(1)$. It is important to identify the pairing state with an internal degree of freedom of Cooper pairs in order to examine exotic phenomena in unconventional superconductors (SCs). Furthermore, the identification gives a clue to the pairing mechanism and offers the future application of unconventional SCs to new superconducting devices.

Recently, locally noncentrosymmetric (LNCS) superconducting systems are regarded as a new family of exotic SCs [4,5]. These systems are found in various real crystalline materials, such as the heavy-fermion superlattice $CeCoIn_5/YbCoIn_5$ [6], the pnictide SC SrPtAs [7], the layered transition-metal dichalcogenides [8], and so on. A staggered antisymmetric spin-orbit coupling (ASOC) due to the local noncentrosymmetricity appears in the LNCS system with global inversion symmetry, as the uniform ASOC appears in the noncentrosymmetric (NCS) system without global inversion symmetry. In LNCS systems, the sublattice structure plays an important role in the internal structure of the Cooper pair [9]. In a multilayered system, Maruyama *et al.* showed that superconducting properties continuously change from the isolated NCS layers to the correlated LNCS multilayer with increasing interlayer coupling, in terms of the study of the spin susceptibility in the superconducting state [10].

Exotic superconducting phases called the pair-density-wave (PDW) phase [11] and the complex-stripe phase [12] were theoretically predicted to stabilize in multilayered systems in a high magnetic field when the paramagnetic depairing effect is dominant. Indeed, experimental results in $CeCoIn_5(n)/YbCoIn_5(5)$ epitaxial superlattices suggested that some exotic superconducting states might be realized at high magnetic fields [13]. A numerical calculation demonstrated that the PDW phase stabilizes at low temperatures and high magnetic fields perpendicular to the layers through the s-wave pairing interaction, layer-dependent Rashba ASOC, and Zeeman magnetic field [11]. In the PDW state, the phase of the superconducting order parameter modulates layer by layer [11]. For instance, in the simplest model for multilayered systems, namely, bilayer systems, the order parameter Δ changes its phase by π between layers, $(\Delta_1,\Delta_2) = (\Delta, -\Delta)$. Such unusual stacking of the order parameter is in sharp contrast to the conventional BCS state, where the order parameter is uniform, $(\Delta_1,\Delta_2) = (\Delta,\Delta)$. In real materials, vortices appear in the high magnetic field, although previous studies neglected them [11,12]. When the vortex density is not large, the phase modulation around vortices does not seriously affect the phase modulation between the stacked layers. Thus, the vortices induced by the orbital effect do not play a crucial role in the stability of the PDW phase [11]. It is, however, important to investigate the vortex state since the excitations around vortex cores dominate transport and thermodynamic properties. Moreover, the observation of quasiparticle states around a vortex core gives us different types of information to identify the pairing state. The quasiparticle states can be

*Present address: Department of Physics, Sungkyunkwan University, Suwon 16419, Korea; y.higashi@skku.edu

†Present address: Department of Physics, Gakushuin University, Tokyo 171-8588, Japan.

‡Present address: Department of Physics, Graduate School of Science, Kyoto University, Kyoto 606-8502, Japan.

experimentally studied through the local quasiparticle density of states (LDOS), which is obtained by scanning tunneling microscopy/spectroscopy (STM/STS) experiments with high spatial and energy resolutions.

The first STM/STS measurement of the vortex-core states focusing on the NCS superconductivity was conducted on the β-pyrochlore osmate KOs_2O_6 [14]. Recently, the vortex bound states were experimentally explored also in NCS BiPd by STM/STS [15]. A theoretically predicted spectroscopic feature of the parity-mixed superconducting state due to the lack of an inversion center is a two-gap structure of quasiparticle spectra in the bulk [16], but no distinct spectroscopic evidence was observed in these experiments. In recent years, however, vortex-core states in materials with strong spin-orbit coupling (SOC) have been measured by STM/STS in the context of topological superconductivity [17–19]. Thus, it is an intriguing study to elucidate the effect of SOC on the electronic structure around a quantum vortex in exotic SCs.

This paper is organized as follows. First, in Sec. II, we introduce multilayered superconducting systems. In Sec. III, we sketch the quasiclassical Green's function method with the use of the perturbative method for SOC. Then, we demonstrate that the electronic structure around a vortex core in the PDW pairing state is drastically different from that in the BCS state in Sec. IV. We also elucidate the key roles of SOC in the difference in LDOS structure around a core between the BCS and PDW states. In Sec. V, we discuss energy spectra in the bulk and clarify the relation to the vortex bound states. In Sec. VI, we discuss further the properties of the PDW state and its realization in real crystalline materials. A brief summary is given in Sec. VII.

II. MULTILAYERED SYSTEM

In this paper, we consider superconductivity in a bilayer system (the number of layers is $N = 2$) with a layer-dependent ASOC, $(\alpha_1,\alpha_2) = (\alpha, -\alpha)$, the Zeeman field, and interlayer hopping. Throughout the paper, we use the units in which $\hbar = k_B = c = 1$. The normal state is described by the following Hamiltonian including a spin degree of freedom:

$$\mathscr{H}_0 = \sum_{s,s',m} \int d\boldsymbol{r} \int d\boldsymbol{r}' \psi^\dagger_{sm}(\boldsymbol{r}) h_{ss'm}(\boldsymbol{r},\boldsymbol{r}', -i\nabla_{\boldsymbol{r}'}) \psi_{s'm}(\boldsymbol{r}') + t_\perp \sum_{s,\langle m,m'\rangle} \int d\boldsymbol{r} \psi^\dagger_{sm}(\boldsymbol{r}) \psi_{sm'}(\boldsymbol{r}), \tag{1}$$

$$h_{ss'm}(\boldsymbol{r},\boldsymbol{r}', -i\nabla_{\boldsymbol{r}'}) = \delta_{ss'}\delta(\boldsymbol{r}-\boldsymbol{r}')\xi(\boldsymbol{r}', -i\nabla_{\boldsymbol{r}'}) - \delta(\boldsymbol{r}-\boldsymbol{r}')\mu_B \boldsymbol{H}\cdot\boldsymbol{\sigma}_{ss'} + \alpha_m \boldsymbol{g}(\boldsymbol{r}-\boldsymbol{r}')\cdot\boldsymbol{\sigma}_{ss'}, \tag{2}$$

where $\psi^\dagger_{sm}(\boldsymbol{r})$ [$\psi_{sm}(\boldsymbol{r})$] is the field operator creating (annihilating) a quasiparticle with the spin s at position $\boldsymbol{r}$ in the mth superconducting layer in the Schrödinger representation and $\xi(\boldsymbol{r}', -i\nabla_{\boldsymbol{r}'}) = [-i\nabla_{\boldsymbol{r}'} + e\boldsymbol{A}(\boldsymbol{r}')]^2/(2m_e) - \mu$ is the free-electron energy dispersion measured from the chemical potential μ with the bare-electron mass m_e, the absolute value of the electron charge e, and the vector potential $\boldsymbol{A}(\boldsymbol{r})$. $t_\perp$ is the interlayer coupling energy. $\langle m,m'\rangle$ indicates the summation over the neighboring layers. μ_B is the magnetic moment of quasiparticles, and $\boldsymbol{H} = (0,0,H)$ is a magnetic field perpendicular to the superconducting layers. $\boldsymbol{\sigma} = (\sigma_x,\sigma_y,\sigma_z)^T$ is the vector representation of the Pauli spin matrix. α_m is the spin-orbit coupling energy in the mth layer, and the orbital vector $\boldsymbol{g}(\boldsymbol{r}-\boldsymbol{r}')$ characterizing the SOC is defined through $\boldsymbol{g}(\boldsymbol{k})$ as

$$\boldsymbol{g}(\boldsymbol{k}) = \int d\bar{\boldsymbol{r}} e^{-i\boldsymbol{k}\cdot\bar{\boldsymbol{r}}} \boldsymbol{g}(\bar{\boldsymbol{r}} = \boldsymbol{r}-\boldsymbol{r}'). \tag{3}$$

Here $\boldsymbol{k}$ denotes the relative wave vector. We consider the Rashba-type SOC in the two-dimensional system described by the orbital vector $\boldsymbol{g}(\boldsymbol{k}) = (-k_y,k_x,0)/k_F$ with the Fermi wave number k_F and $(k_x,k_y) = k(\cos\phi_k, \sin\phi_k)$. ϕ_k is the azimuthal angle.

In this study, we neglect the mixing of Cooper pair wave functions with different parities for simplicity and consider the spin-singlet s-wave pairing. The superconducting order parameter in N-layered systems is expressed as $\hat{\Delta}(\boldsymbol{r}) = \Delta(\boldsymbol{r})i\sigma_y \otimes D$, where D is the $N \times N$ diagonal matrix in the space composed of the layer degree of freedom (band space). In the bilayer system ($N = 2$), $D = \mathrm{diag}(1,s)$, with $s = 1$ (-1) corresponding to the BCS (PDW) state. A symbol $\hat{}$ denotes the $2N \times 2N$ matrix in spin and band space. In this paper, we investigate vortex-core structures by assuming the layer dependence of the order parameter (BCS or PDW state) and leave the discussion of its thermodynamic stability to future studies. Considering a SC with a dominant paramagnetic depairing effect and a large Ginzburg-Landau parameter, we ignore the vector potential. The vortex solution in this situation is studied by self-consistently determining the spatial profile of the pairing potential $\Delta(\boldsymbol{r})$.

III. QUASICLASSICAL THEORY IN MULTILAYERED SYSTEMS

In the PDW state, the order parameter shows a spatial modulation perpendicular to layers in the length scale of the lattice constant, which is much shorter than the characteristic length scale of most SCs. On the other hand, the order parameter varies in the scale of the coherence length within the layer. Therefore, we can develop the quasiclassical theory as follows.

We investigate the electronic structure around a single vortex by means of the quasiclassical theory. As a result of the quasiclassical approximation, the quasiclassical Green's function depends on the center-of-mass coordinate of the Cooper pair $\boldsymbol{r}$, the direction of the relative wave vector (or momentum) of the Cooper pair $\tilde{\boldsymbol{k}} = (\cos\phi_k, \sin\phi_k)$, and the Matsubara frequency for fermions $\omega_n = (2n+1)\pi T$ with the temperature T and an integer n. We define the quasiclassical Green's function as the following $4N \times 4N$ matrix in the Nambu space:

$$\check{g}(\boldsymbol{r},\tilde{\boldsymbol{k}},i\omega_n) = -i\pi \begin{pmatrix} \hat{g}(\boldsymbol{r},\tilde{\boldsymbol{k}},i\omega_n) & i\hat{f}(\boldsymbol{r},\tilde{\boldsymbol{k}},i\omega_n) \\ -i\hat{\bar{f}}(\boldsymbol{r},\tilde{\boldsymbol{k}},i\omega_n) & -\hat{\bar{g}}(\boldsymbol{r},\tilde{\boldsymbol{k}},i\omega_n) \end{pmatrix}. \tag{4}$$

Let us derive the Eilenberger equation with the $4N \times 4N$ matrix quasiclassical Green's function using the perturbation method [20]. In the absence of the Rashba ASOC, Zeeman magnetic field, and interlayer hopping (i.e., $\alpha = \mu_B H = t_\perp = 0$), the FSs have $2N$-fold degeneracy in the normal state. In

this case, one can easily obtain the unperturbed Eilenberger equation expressed as

$$i\boldsymbol{v}_{\rm F}(\tilde{\boldsymbol{k}})\cdot\nabla\check{g}(\boldsymbol{r},\tilde{\boldsymbol{k}},i\omega_n)+[i\omega_n\check{\tau}_3-\check{\Delta}(\boldsymbol{r}),\check{g}(\boldsymbol{r},\tilde{\boldsymbol{k}},i\omega_n)]=\check{0}, \tag{5}$$

where

$$\check{\tau}_3=\begin{pmatrix}\sigma_0\otimes I_{N\times N} & \hat{0}\\ \hat{0} & -\sigma_0\otimes I_{N\times N}\end{pmatrix}, \tag{6}$$

$$\check{\Delta}(\boldsymbol{r})=\begin{pmatrix}\hat{0} & \hat{\Delta}(\boldsymbol{r})\\ -\hat{\Delta}^\dagger(\boldsymbol{r}) & \hat{0}\end{pmatrix}. \tag{7}$$

Here σ_0 and $I_{N\times N}$ are the unit matrices in the spin and band spaces, respectively. The brackets $[\cdots,\cdots]$ are a commutator. We add the Zeeman, Rashba, and interlayer hopping terms into the above equations through self-energy as

$$\check{K}(\tilde{\boldsymbol{k}})=[-\mu_{\rm B}\boldsymbol{H}+\alpha\check{\boldsymbol{g}}(\tilde{\boldsymbol{k}})]\cdot\check{\boldsymbol{S}}+t_\perp(\sigma_0\otimes T_\perp)\otimes\check{\tau}_0, \tag{8}$$

$$\check{\boldsymbol{S}}=\begin{pmatrix}\boldsymbol{\sigma}\otimes I_{N\times N} & \hat{0}\\ \hat{0} & \boldsymbol{\sigma}^*\otimes I_{N\times N}\end{pmatrix}, \tag{9}$$

$$\check{\boldsymbol{g}}(\tilde{\boldsymbol{k}})=\begin{pmatrix}\boldsymbol{g}(\tilde{\boldsymbol{k}})\sigma_0\otimes S_{\rm d} & \hat{0}\\ \hat{0} & \boldsymbol{g}(-\tilde{\boldsymbol{k}})\sigma_0\otimes S_{\rm d}\end{pmatrix}. \tag{10}$$

Here, $T_\perp=\text{offdiag}(1,1)$ and $S_{\rm d}=\text{diag}(1,-1)$; offdiag$(\cdot,\cdot)$ denotes the 2×2 matrix which has only the off-diagonal component in the band space. Thus, we obtain the Eilenberger equation in the $4N\times4N$ matrix form with the self-energy matrix $\check{K}(\tilde{\boldsymbol{k}})$ as

$$\begin{aligned}&i\boldsymbol{v}_{\rm F}(\tilde{\boldsymbol{k}})\cdot\nabla\check{g}(\boldsymbol{r},\tilde{\boldsymbol{k}},i\omega_n)\\&\quad+[i\omega_n\check{\tau}_3-\check{\Delta}(\boldsymbol{r})-\check{K}(\tilde{\boldsymbol{k}}),\check{g}(\boldsymbol{r},\tilde{\boldsymbol{k}},i\omega_n)]=\check{0}.\end{aligned} \tag{11}$$

Since we consider the SC in which the paramagnetic depairing effect is dominant, we incorporate the Zeeman term into the Eilenberger equation. In the presence of the Zeeman term, the Eilenberger equation cannot be decomposed into the two decoupled equations for the spin-split Fermi surface, although we can do so at $H=0$ by using the band basis representation [21]. Therefore, we take the orbital basis, in which the spin quantization axis is parallel to the z axis. In the orbital basis, we can transform Eq. (3.8) into the two matrix Riccati equations, regarding $\check{K}(\tilde{\boldsymbol{k}})$ as the *self-energy* [22]:

$$\begin{aligned}&\boldsymbol{v}_{\rm F}(\tilde{\boldsymbol{k}})\cdot\nabla\hat{a}_0+2\omega_n\hat{a}_0+\hat{a}_0\hat{\Delta}_0^\dagger\hat{a}_0-\hat{\Delta}_0\\&\quad+i\left(\hat{K}_{11}^0\hat{a}_0+\hat{a}_0\hat{K}_{22}^0\right)=\hat{0},\end{aligned} \tag{12}$$

$$\begin{aligned}&\boldsymbol{v}_{\rm F}(\tilde{\boldsymbol{k}})\cdot\nabla\hat{b}_0-2\omega_n\hat{b}_0-\hat{b}_0\hat{\Delta}_0\hat{b}_0+\hat{\Delta}_0^\dagger\\&\quad-i\left(\hat{b}_0\hat{K}_{11}^0+\hat{K}_{22}^0\hat{b}_0\right)=\hat{0}.\end{aligned} \tag{13}$$

Here we define $\check{K}(\tilde{\boldsymbol{k}})=\text{diag}(\hat{K}_{11}(\tilde{\boldsymbol{k}}),\hat{K}_{22}(\tilde{\boldsymbol{k}}))$ in the Nambu space with $\hat{K}_{11}(\tilde{\boldsymbol{k}})\equiv-\mu_{\rm B}H\sigma_z\otimes I_{N\times N}+\alpha\boldsymbol{g}(\tilde{\boldsymbol{k}})\cdot\boldsymbol{\sigma}\otimes S_{\rm d}+t_\perp\sigma_0\otimes T_\perp$ and $\hat{K}_{22}(\tilde{\boldsymbol{k}})\equiv-\mu_{\rm B}H\sigma_z\otimes I_{N\times N}-\alpha\boldsymbol{g}(\tilde{\boldsymbol{k}})\cdot\boldsymbol{\sigma}^*\otimes S_{\rm d}+t_\perp\sigma_0\otimes T_\perp$, and we introduce the following expressions: $\hat{a}=\hat{a}_0(i\sigma_y\otimes I_{N\times N})$, $\hat{b}=(i\sigma_y\otimes I_{N\times N})\hat{b}_0$, $\hat{K}_{11}=\hat{K}_{11}^0$, $\hat{K}_{22}=(-\sigma_y\otimes I_{N\times N})\hat{K}_{22}^0(\sigma_y\otimes I_{N\times N})$, $\hat{\Delta}=\hat{\Delta}_0(i\sigma_y\otimes I_{N\times N})$, and $\hat{\Delta}^\dagger=(i\sigma_y\otimes I_{N\times N})\hat{\Delta}_0^\dagger$. $\hat{a}$ and $\hat{b}$ are the former Riccati parameters.

Using the pairing interaction adopted by Ref. [23], the gap equation for the spin-singlet component is obtained as [1]

$$\begin{aligned}\Delta(\boldsymbol{r})=\lambda\pi T\frac{1}{2}\sum_{-n_{\rm c}(T)-1<n<n_{\rm c}(T)}\sum_{s_1's_2'}(i\sigma_y)^\dagger_{s_2's_1'}\\\times\langle f^0_{s_1's_2'}(\boldsymbol{r},\tilde{\boldsymbol{k}}',i\omega_n)(i\sigma_y)_{s_1's_2'}\rangle_{\tilde{\boldsymbol{k}}'},\end{aligned} \tag{14}$$

where $\langle\cdots\rangle_{\tilde{\boldsymbol{k}}}$ is the average on the Fermi surface. We use the following coupling constant obtained in the bulk at $\alpha=\mu_{\rm B}H=t_\perp=0$:

$$\frac{1}{\lambda}=\ln\left(\frac{T}{T_{\rm c0}}\right)+\sum_{0\leqslant n<n_{\rm c}(T)}\frac{2}{2n+1}, \tag{15}$$

where $T_{\rm c0}$ is the superconducting transition temperature at $\alpha=\mu_{\rm B}H=t_\perp=0$ and $n_{\rm c}(T)=(\omega_{\rm c}/\pi T-1)/2$. We fix the cutoff frequency to $\omega_{\rm c}=7\pi T_{\rm c0}$. The LDOS per spin and layer is given by

$$N(E,\boldsymbol{r})=-\frac{N_{\rm F}}{2N}\frac{1}{\pi}\langle\text{Im}[\text{Tr}\hat{g}(\boldsymbol{r},\tilde{\boldsymbol{k}},i\omega_n\to E+i\eta)]\rangle_{\tilde{\boldsymbol{k}}}. \tag{16}$$

$N_{\rm F}$ is the density of states (DOS) per spin and layer at the Fermi level in the normal state. E and η are the real energy and the energy-smearing factor, respectively.

IV. ELECTRONIC STRUCTURE AROUND A VORTEX CORE

In this section, we clarify the difference in the electronic structure around a vortex core between the BCS and PDW states. We show the self-consistently calculated spatial profiles of the pair potential and LDOS. The presence or absence of the zero-energy peak (ZEP) in LDOS is demonstrated. We fix the temperature, the Zeeman field, and the interlayer hopping to $T/T_{\rm c0}=0.1$, $\mu_{\rm B}H/T_{\rm c0}=1.5$, and $t_\perp/T_{\rm c0}=1$, respectively, unless we state otherwise.

A. Pair potential

Let us discuss the spatial profiles of the pair potential amplitude $|\Delta(r)|$ around a vortex.

First, we discuss the Zeeman magnetic field dependence of the vortex-core radius for $\alpha/T_{\rm c0}=2$. The vortex-core radius is defined as [24–26]

$$\xi_1(H)=\Delta(H,r=r_{\rm c})/\lim_{r\to0}\frac{\Delta(H,r)}{r}, \tag{17}$$

where we set $r_{\rm c}=10\xi_0$. As shown in Fig. 1, the vortex-core radius $\xi_1(H)$ in the BCS state diverges at the critical magnetic field due to the paramagnetic depairing. Because the PDW state is more robust against the paramagnetic depairing than the BCS state, the critical magnetic field of the PDW state is higher than that of the BCS state. Indeed, Fig. 1 shows the divergence of $\xi_1(H)$ in the PDW state at a higher magnetic field. Then, the vortex core suddenly shrinks at the first-order BCS-PDW transition which occurs at $\mu_{\rm B}H/T_{\rm c0}\simeq1.8$ [27]. This sudden shrinkage of the vortex core originates from the difference in the superconducting gap between the BCS and PDW states. At the transition magnetic field, the superconducting gap is larger in the PDW state than in the BCS state [11].

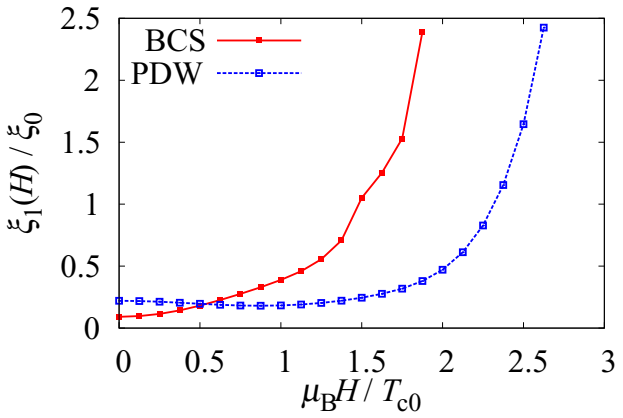

FIG. 1. Zeeman magnetic field dependences of the vortex-core radius $\xi_1(H)$ for $\alpha/T_{c0} = 2$. We set $T/T_{c0} = 0.1$ and $t_\perp/T_{c0} = 1$.

Next, we discuss the effect of SOC on the spatial profiles of the pair potential. The pair potential amplitude $|\Delta(r)|$ significantly depends on the strength of the SOC, as shown in Fig. 2. The horizontal axis indicates the radial distance from the vortex center ($r = 0$) normalized by the coherence length $\xi_0 = v_F/T_{c0}$ for $\alpha = \mu_B H = t_\perp = 0$. The BCS state [Fig. 2(a)] is destabilized by the paramagnetic depairing for a small SOC $\alpha/T_{c0} \lesssim 1$ because we adopt a magnetic field larger

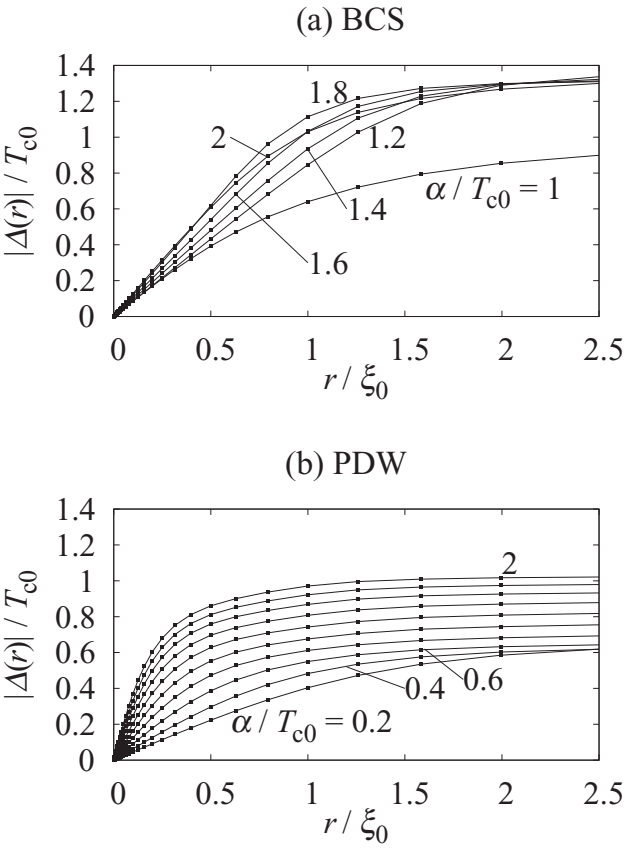

FIG. 2. Spatial profiles of the pair potential amplitudes $|\Delta(r)|$ for the (a) BCS and (b) PDW states. The horizontal axis represents the radial distance from a vortex center $r = 0$. We set $T/T_{c0} = 0.1$ and $t_\perp/T_{c0} = 1$. SOC strength is indicated for each curve. $\alpha/T_{c0} = 0.2$–2 is increased from the bottom to the top by a 0.2 step in (b).

than the conventional Pauli limit. On the other hand, the PDW state is robust against the magnetic field since the paramagnetic depairing is suppressed [10] and the PDW state survives even when the SOC is small $\alpha/T_{c0} \lesssim 1$ [Fig. 2(b)]. It is shown that both BCS and PDW states are stabilized by the SOC in the high magnetic field ($\mu_B H/T_{c0} = 1.5$). In the PDW state, the pair potential amplitude gets larger monotonically with increasing SOC strength α. This is because the PDW state can be mapped onto the two-dimensional Rashba SC with the use of the mirror symmetry, which will be discussed later, and then the Rashba-type SOC locks the spin quantization axis within the x-y plane to suppress the paramagnetic depairing effect. In contrast, in the BCS state, the pair potential amplitude shows an unusual nonmonotonic behavior with increasing SOC strength.

An intriguing feature is seen in the vortex-core radius. As shown in Fig. 2(b), the core radius in the PDW state is smaller than that in the BCS state, in accordance with Fig. 1. This feature becomes prominent with increasing SOC strength.

B. Local density of states

We here discuss the energy and spatial dependence of the LDOS around a vortex in the BCS and PDW states and clarify the change in the electronic structure at the BCS-PDW transition. We fix the Zeeman magnetic field and the SOC strength to $\mu_B H/T_{c0} = 1.5$ and $\alpha/T_{c0} = 2$, respectively. The self-consistent solutions for the gap equation displayed in Fig. 2 are used to calculate the LDOS. In the BCS states, as shown in Fig. 3(a), the zero-energy vortex bound states split into the four peaks due to the interlayer hopping and the Zeeman field. On the other hand, in the PDW state, a large quasiparticle DOS appears at the zero energy [see Fig. 3(b)]. This is quite a contrast to the LDOS structure in the BCS state.

When we consider the PDW state in the absence of the SOC (the PDW state is indeed unstable in the absence of the SOC), the four LDOS peaks appear as in the BCS state due to the interlayer hopping and the Zeeman field. The magnetic field dependence of the LDOS is also similar to that in the BCS state.

Thus, the contrasting behaviors between the PDW and BCS states in Fig. 3 result from the SOC. One might speculate that the two peaks in the LDOS at $\alpha = 0$ get combined with increasing SOC strength. However, we should notice another origin of the appearance of the zero-energy vortex bound states in the PDW state, which is described next.

C. Emergent zero-energy peak by spin-orbit coupling

In this section, we show the SOC strength dependence of the vortex bound states. As we discussed in the previous section, in the absence of the SOC, the quasiparticle structure around the vortex core is similar between the PDW and BCS states. On the other hand, in the presence of the SOC, the internal structure of Cooper pairs manifests itself in the quasiparticle structure [9–11]. Indeed, the zero-energy quasiparticle state appears around a vortex core in the PDW state as a result of the sign change of the order parameter between layers [Fig. 3(b)], although the ZEP splits in the BCS state. In order to elucidate the effect of the SOC on the quasiparticle structure, we show in Fig. 4 the LDOS at the vortex center for various SOC strengths.

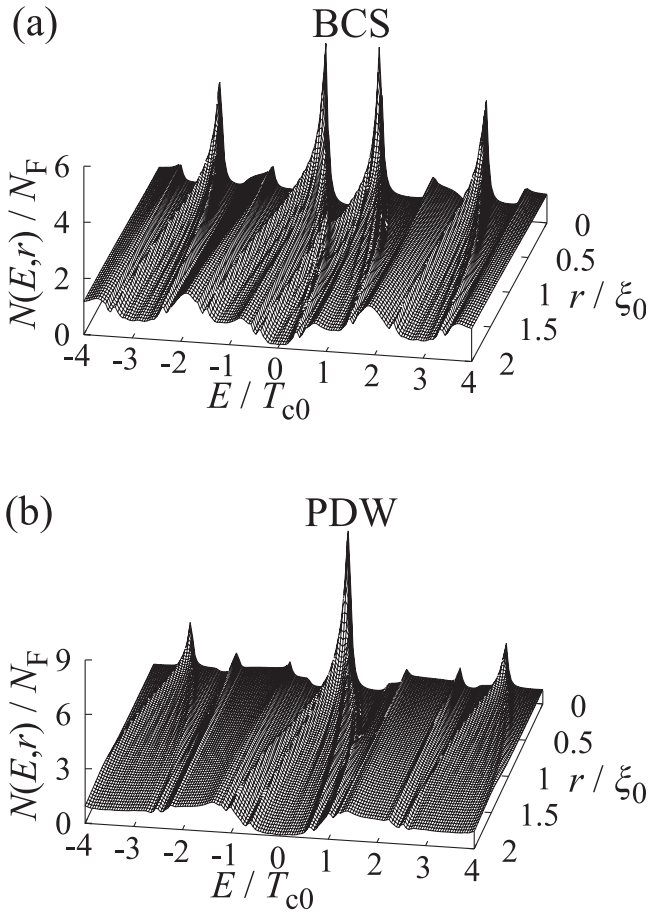

FIG. 3. LDOS $N(E,r)$ (a) in the BCS state and (b) in the PDW state. The Zeeman field is set to $\mu_B H/T_{c0} = 1.5$, and the SOC is $\alpha/T_{c0} = 2$ for both pairing states. Other parameters are $T/T_{c0} = 0.1$, $t_\perp/T_{c0} = 1$, and $\eta = 0.05T_{c0}$.

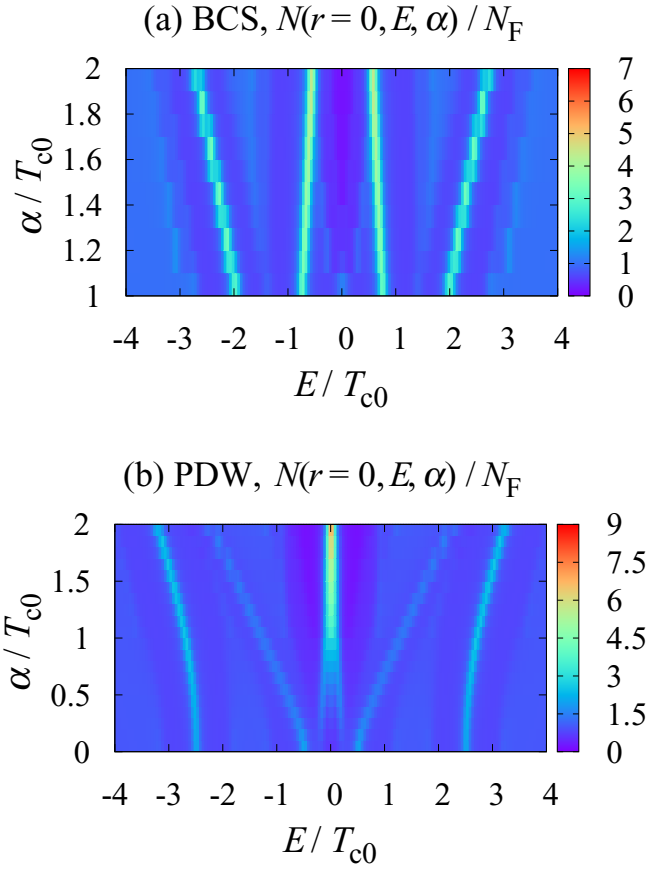

FIG. 4. The energy and SOC strength dependences of the LDOS at the vortex center $N(r=0,E,\alpha)$ (a) in the BCS state and (b) in the PDW state for $\mu_B H/T_{c0} = 1.5$. Other parameters are $T/T_{c0} = 0.1$, $t_\perp/T_{c0} = 1$, and $\eta = 0.05T_{c0}$.

For the parameters in Fig. 4, the BCS state is completely suppressed due to the paramagnetic depairing for $\alpha/T_{c0} \lesssim 1$. Thus, we show the results for $\alpha/T_{c0} \geqslant 1$. As shown in Fig. 4(a), Andreev bound states have a finite energy almost independent of the SOC strength. The peaks in the low-energy region shift a little to lower energy with increasing SOC strength, whereas those in the high-energy region move to higher energy.

On the other hand, in the PDW state, the ZEP in LDOS gradually develops with increasing SOC strength [see Fig. 4(b)]. At $\alpha/T_{c0} = 2$, the LDOS at the vortex center clearly shows the ZEP, which was already shown in Fig. 3(b). Thus, the SOC plays a crucial role in the contrasting quasiparticle structure around a vortex core between the BCS and PDW states. The SOC is much larger than the superconducting gap in most NCS and LNCS systems, and thus, the condition $\alpha/T_{c0} \gg 1$ is satisfied. Therefore, the zero-energy bound states will appear around the vortex core when the PDW state is stabilized in the magnetic field.

Although the vortex-core states in the BCS state show Zeeman splitting, the ZEP in the PDW state is robust against the Zeeman field. This result can be viewed as a result of the suppression of the paramagnetic depairing effect in the PDW state. An indication of the suppression of the paramagnetic depairing effect is obtained by calculating the c-axis spin susceptibility in the superconducting state. As shown in Ref. [10], the spin susceptibility is not decreased by the PDW order (see Figs. 2 and 11 in Ref. [10]). This indicates that the Zeeman field does not suppress the superconducting state and does not split the ZEP. Another consequence of the suppression of the paramagnetic depairing effect is the particle-hole symmetry in the mirror subsector in the PDW state [28]. This aspect is discussed in Sec. V.

In the next section, we show the energy spectra in the bulk to clarify the effect of the SOC on the energy dispersion. We also discuss the relation between the vortex bound states and the bulk energy spectra.

V. ENERGY SPECTRA IN THE BULK

In this section, we investigate the effects of the SOC on the energy spectra in the bulk and discuss the relation between the bulk superconducting gap and the vortex bound states. We diagonalize the following 8×8 Bogoliubov–de Gennes (BdG) Hamiltonian to obtain the energy spectra:

$$\check{\mathscr{H}}_{\rm BdG} = \begin{pmatrix} \hat{\mathscr{H}}_0(\boldsymbol{k}) & \hat{\Delta} \\ \hat{\Delta}^\dagger & -\hat{\mathscr{H}}_0^*(-\boldsymbol{k}) \end{pmatrix}, \tag{18}$$

$$\hat{\mathscr{H}}_0(\boldsymbol{k}) = \begin{pmatrix} h_1(\boldsymbol{k}) & t_\perp\sigma_0 \\ t_\perp\sigma_0 & h_2(\boldsymbol{k}) \end{pmatrix}, \tag{19}$$

where $h_m(\boldsymbol{k}) = \xi(k)\sigma_0 + \alpha_m \boldsymbol{g}(\boldsymbol{k})\cdot\boldsymbol{\sigma} - \mu_B \boldsymbol{H}\cdot\boldsymbol{\sigma}$. We adopt the isotropic dispersion relation $\xi(k) = k^2/2m_e - \mu$ and the orbital vector $\boldsymbol{g}(\boldsymbol{k}) = (-k_y, k_x, 0)/k_{F0} = (k/k_{F0})(-\sin\phi_k, \cos\phi_k, 0)$ in two-dimensional layers. k_{F0} is the Fermi wave number for $\alpha = \mu_B H = t_\perp = 0$.

In most NCS and LNCS systems, the SOC strength α is much larger than the superconducting gap energy at zero temperature Δ_0 and much smaller than the Fermi energy E_F. Thus, the SCs are in the quasiclassical regime, namely, $k_F\xi_0 \sim E_F/\Delta_0 \gg 1$, and the energy scale of the SOC may satisfy the condition $\Delta_0 \ll \alpha \ll E_F$. However, we adopt parameters in the quantum limit regime ($E_F/\Delta_0 = 5$) for visibility in the figures. We confirmed that the following discussions are correct also in the quasiclassical regime.

A. Absence of spin-orbit coupling

The superconducting energy gap can be viewed as a hybridization gap between electron and hole bands in a certain basis. We study the s-wave BCS state and PDW state in this section. As carried out in Refs. [28,29], the BdG Hamiltonian is block diagonalized by using the mirror symmetry. Then, the interlayer hopping $t_\perp$ is taken into account through an effective Zeeman magnetic field $h_\pm\sigma_z = (\mu_B H \pm t_\perp)\sigma_z$ [28] in a subsector Hamiltonian. As a result of the lifting of fourfold degeneracy due to the effective Zeeman field, four energy bands appear in both electron and hole branches. Figures 5(a) and 5(b) show the normal-state energy bands $\pm E_{2\uparrow}(k) = \pm[\xi(k) - h_+]$, $\pm E_{1\uparrow}(k) = \pm[\xi(k) - h_-]$, $\pm E_{2\downarrow}(k) = \pm[\xi(k) + h_-]$, and $\pm E_{1\downarrow}(k) = \pm[\xi(k) + h_+]$ from bottom (top) to top (bottom) at $k = 0$ for the electron (hole) bands. The blue and red lines show the energy bands for $m = 2$ and 1, respectively. We choose the parameters $\mu_B H/T_{c0} = 1.5$ and $t_\perp/T_{c0} = 1$ ($\mu_B H/E_{F0} = 0.3$ and $t_\perp/E_{F0} = 0.2$).

As investigated in Ref. [10] and pointed out in Ref. [11], in the absence of the SOC, intraband quasiparticle states form the Cooper pairs in the BCS state, whereas interband pairing states are realized in the PDW state. In Figs. 5(a) and 5(b), arrows show the positions of superconducting gap in the BCS and PDW states, respectively. In the BCS state four spectral gaps open via the intraband spin-singlet Cooper pairing [Fig. 5(a)]. In the PDW state four gaps are induced by the interband spin-singlet pairing [Fig. 5(b)]. The superconducting gaps are symmetric with respect to E_F because of the particle-hole symmetry. In both BCS and PDW states the superconducting gaps are shifted away from E_F. In the BCS state at $\alpha = 0$ the shift is due to the paramagnetic depairing effect, and indeed, the BCS state is completely destroyed due to the paramagnetic depairing at $\mu_B H/T_{c0} = 1.5$. On the other hand, the PDW state is unstable at $\alpha = 0$ because the interband pairing gives rise to the superconducting gap away from the Fermi energy even at $H = 0$.

B. Presence of spin-orbit coupling

In the presence of the SOC, the interband Cooper pairs are formed in the BCS state, whereas the intraband Cooper pairs as well as the interband Cooper pairs are formed in the PDW state. Figures 6(a) and 6(b) depict the electron (hole) band in the normal state from bottom (top) to top (bottom) at $k = 0$; $\pm E_+^{\rm Low}(k) = \pm[\xi(k) - E_+]$, $\pm E_-^{\rm Low}(k) = \pm[\xi(k) - E_-]$, $\pm E_-^{\rm Upp}(k) = \pm[\xi(k) + E_-]$, and $\pm E_+^{\rm Upp}(k) = \pm[\xi(k) + E_+]$, with $E_\pm = \sqrt{h_\pm^2 + (\tilde{k}\alpha)^2}$ and $\tilde{k} = k/k_{F0}$. Unlike in Fig. 5, the blue and red lines in Figs. 6 indicate the energy spectra of the subsector Hamiltonian described by the effective magnetic fields h_- and h_+, respectively.

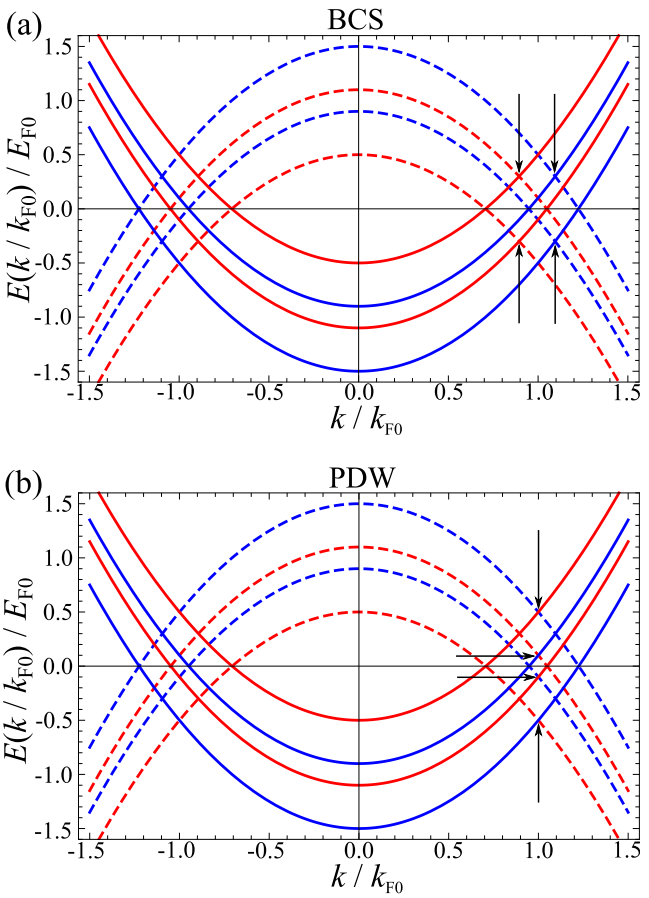

FIG. 5. Normal-state energy spectra at $\alpha = 0$. Arrows indicate the intersections of electron and hole bands which form Cooper pairs in (a) the BCS state and (b) the PDW state. The horizontal axis denotes the wave number normalized by k_{F0}. Other parameters are set to $\mu_B H/E_{F0} = 0.3$, $t_\perp/E_{F0} = 0.2$, and $\mu/E_{F0} = 1$, with $E_{F0} = k_{F0}^2/2m_e$.

For multilayered Rashba SCs or two-dimensional Rashba SCs in the presence of both the SOC and Zeeman field, the band representation of the superconducting order parameter has been obtained by several authors [10,30–32]. By carrying out the unitary transformation, the band representation of the order parameter in the BCS state is given in the band basis as

$$\hat{\Delta}_{\rm BCS}^{\rm b}(\boldsymbol{k}) = \hat{U}_k^\dagger \hat{\Delta}_{\rm BCS}\hat{U}_{-k}^* = \begin{pmatrix} 0_{2\times2} & \Delta_{\rm BCS}^{\rm b-+}(\boldsymbol{k}) \\ \Delta_{\rm BCS}^{\rm b+-}(\boldsymbol{k}) & 0_{2\times2} \end{pmatrix}, \quad (20)$$

$$\Delta_{\rm BCS}^{\rm b-+}(\boldsymbol{k}) = \frac{i\alpha\tilde{k}e^{-i\phi_k}\Delta}{2\sqrt{E_-E_+}} \times \begin{pmatrix} -\frac{E_-+h_-+E_++h_+}{\sqrt{(E_-+h_-)(E_++h_+)}} & \frac{E_-+h_--(E_+-h_+)}{\sqrt{(E_-+h_-)(E_+-h_+)}} \\ \frac{-(E_--h_-)+E_++h_+}{\sqrt{(E_--h_-)(E_++h_+)}} & \frac{E_--h_-+E_+-h_+}{\sqrt{(E_--h_-)(E_+-h_+)}} \end{pmatrix}, \quad (21)$$

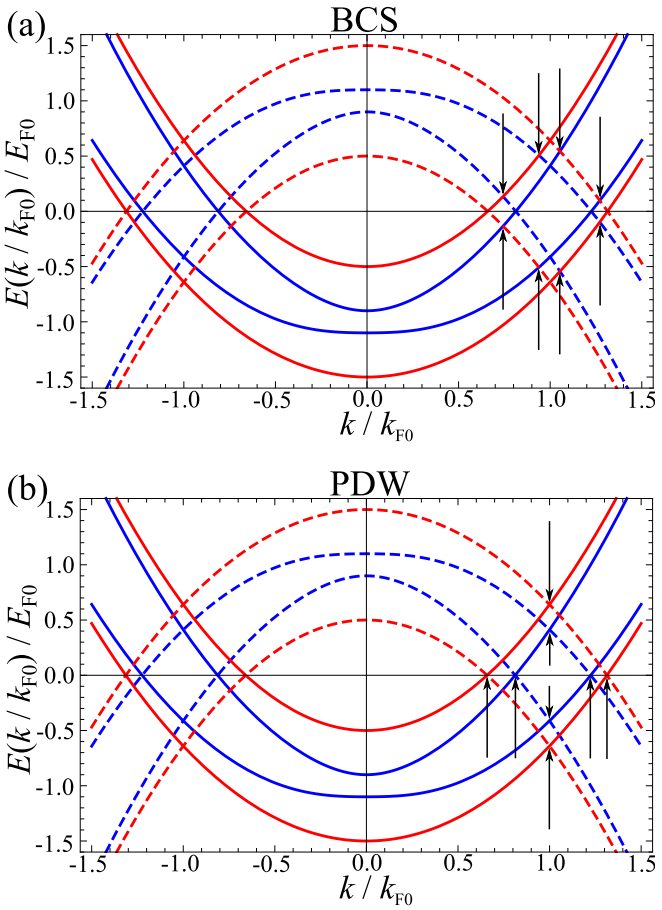

FIG. 6. Normal-state energy spectra at $\alpha/E_{F0} = 0.4$. Arrows indicate the intersections of electron and hole bands which form Cooper pairs in (a) the BCS state and (b) the PDW state. The horizontal axis denotes the wave number normalized by k_{F0}. Other parameters are set to $\mu_B H/E_{F0} = 0.3, t_\perp/E_{F0} = 0.2$, and $\mu/E_{F0} = 1$, with $E_{F0} = k_{F0}^2/2m_e$.

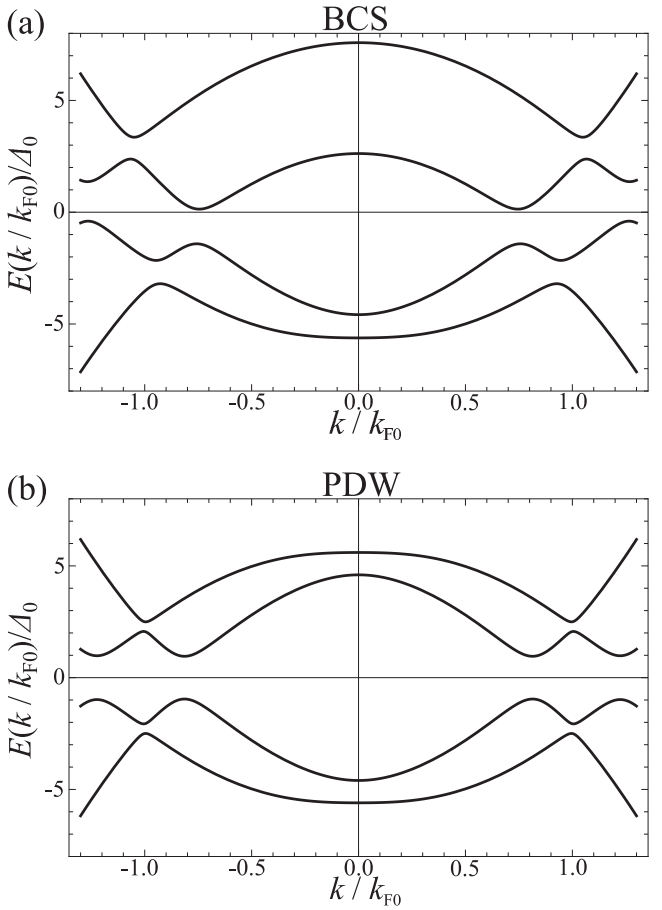

FIG. 7. Energy spectra of (a) the mirror subsector Hamiltonian in the BCS state and (b) that with h_- in the PDW state for $\alpha/\Delta_0 = 2$. The superconducting gap energy is set to $|\Delta|/\Delta_0 = 1$. Other parameters are set to $\mu_B H/\Delta_0 = 1.5, t_\perp/\Delta_0 = 1$, and $E_F/\Delta_0 = 5$.

$$\Delta_{\rm BCS}^{\rm b+-}(\boldsymbol{k}) = \frac{i\alpha\tilde{k}e^{-i\phi_k}\Delta}{2\sqrt{E_-E_+}} \times \begin{pmatrix} -\frac{E_-+h_-+E_++h_+}{\sqrt{(E_-+h_-)(E_++h_+)}} & \frac{-(E_--h_-)+E_++h_+}{\sqrt{(E_--h_-)(E_++h_+)}} \\ \frac{E_-+h_--(E_+-h_+)}{\sqrt{(E_-+h_-)(E_+-h_+)}} & \frac{E_--h_-+E_+-h_+}{\sqrt{(E_--h_-)(E_+-h_+)}} \end{pmatrix}. \tag{22}$$

Here, $\hat{U}_k$ is the unitary matrix diagonalizing $\hat{\mathscr{H}}_0(\boldsymbol{k})$. Similarly, the band representation of the order parameter in the PDW state is obtained as

$$\hat{\Delta}_{\rm PDW}^{\rm b}(\boldsymbol{k}) = \hat{U}_k^\dagger \hat{\Delta}_{\rm PDW} \hat{U}_{-k}^* = \begin{pmatrix} \Delta_{\rm PDW}^{\rm b-}(\boldsymbol{k}) & 0_{2\times2} \\ 0_{2\times2} & \Delta_{\rm PDW}^{\rm b+}(\boldsymbol{k}) \end{pmatrix}, \tag{23}$$

$$\Delta_{\rm PDW}^{\rm b-}(\boldsymbol{k}) = \frac{ie^{-i\phi_k}\Delta}{E_-}\begin{pmatrix} -\alpha\tilde{k} & h_- \\ h_- & \alpha\tilde{k} \end{pmatrix}, \tag{24}$$

$$\Delta_{\rm PDW}^{\rm b+}(\boldsymbol{k}) = \frac{ie^{-i\phi_k}\Delta}{E_+}\begin{pmatrix} -\alpha\tilde{k} & h_+ \\ h_+ & \alpha\tilde{k} \end{pmatrix}. \tag{25}$$

The spectral gap corresponding to each component of the order parameter is indicated by arrows in Fig. 6. We notice that the superconducting gaps open at eight intersections of the electron and hole bands. The feature is different from that at $\alpha = 0$. Thus, the effect of the SOC on the internal structure of Cooper pairs is clarified by using the band representation.

First, in the BCS state [Fig. 6(a)], the superconducting gap does not open just at E_F [$E(k) = 0$]. In order to clarify this point, in Fig. 7(a), we show the energy spectra of a mirror subsector of the block-diagonalized BdG Hamiltonian in the BCS superconducting state. We now understand that the particle-hole asymmetry in the subsector Hamiltonian leads to the shift of the superconducting-gap center from E_F. This is because of the even mirror parity of the BCS state. The other mirror subsector also gives the energy spectra without particle-hole symmetry. When the superconducting gap opens in the bulk, quasiparticle bound states (Andreev bound states) are formed at the core of a singly quantized vortex around the superconducting gap center. Thus, in the BCS state, the energy of Andreev bound states at the vortex core shifts from E_F to a finite energy, leading to the splitting of the ZEP demonstrated in Fig. 3(a).

Next, in the PDW state, the superconducting gaps open at E_F, as shown by arrows in Fig. 6(b). Because of the odd mirror

parity in the PDW state, particle-hole symmetry is preserved in the subsector Hamiltonian [28,29]. Indeed, Fig. 7(b) shows particle-hole symmetry in the energy spectra for a mirror subsector of the block-diagonalized BdG Hamiltonian. The particle-hole symmetry preserved in the subsector allows the Cooper pairs formed by quasiparticles at $E_{\rm F}$. In Fig. 6(b), four arrows indicate the Cooper pairing at $E_{\rm F}$, which is caused by the diagonal component of $\hat{\Delta}^{\rm b}_{\rm PDW}(\boldsymbol{k})$. The appearance of the diagonal components indicates the intraband Cooper pairs induced by the SOC. The inner and outer two arrows at $E_{\rm F}$ in Fig. 6(b) show the pairing states in the mirror subsector with h_- and h_+ [diagonal components of $\Delta^{\rm b-}_{\rm PDW}(\boldsymbol{k})$ and $\Delta^{\rm b+}_{\rm PDW}(\boldsymbol{k})$], respectively. The four arrows far from $E_{\rm F}$ show the interband pairing state described by the off-diagonal components of $\Delta^{\rm b-}_{\rm PDW}(\boldsymbol{k})$ and $\Delta^{\rm b+}_{\rm PDW}(\boldsymbol{k})$. As illustrated in the discussion above, in the PDW state four arrows indicate the Cooper pairing at $E_{\rm F}$, which is caused by the diagonal component of $\hat{\Delta}^{\rm b}_{\rm PDW}(\boldsymbol{k})$. Correspondingly, at the vortex core, the ZEP of vortex bound states appears, as already shown in Fig. 3(b).

The two-gap feature of the quasiparticle spectrum in Fig. 3(b) is also naturally understood by the band representation of the order parameter. The bulk amplitudes of the intraband order parameter in subsectors with effective magnetic fields h_- and h_+ are $|\Delta^{\rm b-}_{\rm PDW}(\boldsymbol{k})| = |\alpha\tilde{k}\Delta/E_-|$ and $|\Delta^{\rm b+}_{\rm PDW}(\boldsymbol{k})| = |\alpha\tilde{k}\Delta/E_+|$ $[|\Delta^{\rm b-}_{\rm PDW}(\boldsymbol{k})| > |\Delta^{\rm b+}_{\rm PDW}(\boldsymbol{k})|]$, respectively. Thus, the two gap edges at low and high energies near $E_{\rm F}$ in Fig. 3(b) correspond to $|\Delta^{\rm b+}_{\rm PDW}(\boldsymbol{k})|$ and $|\Delta^{\rm b-}_{\rm PDW}(\boldsymbol{k})|$, respectively. We note that the two-gap feature in Fig. 3(b) does not stem from the parity mixing of the order parameter, which is neglected in the present work.

VI. DISCUSSION

A. Possible realization in real crystalline materials

We here discuss the possible realization of the PDW ground state in real crystalline materials in the presence of vortices in a high magnetic field. In order to examine if the PDW state stabilizes in a high magnetic field, one needs to evaluate numerically the free energy in the vortex lattice state by employing the Brandt-Pesch-Tewort approximation or a full numerical calculation to solve quasiclassical equations. Although we leave the evaluation of the free energy in the vortex lattice state for a future work, the PDW state is stable in the vortex lattice state in the situation discussed below.

Since the spatial modulation of the order parameter due to vortices occurs within the x-y plane, this modulation does not affect seriously the phase modulation along the z axis specifying the PDW state if the density of vortices is not large. In heavy-fermion compounds, a large effective electron mass gives rise to a short coherence length and a large orbital limit of the upper critical field $H^{\rm orb}_{\rm c2}$. We consider the high-magnetic-field region where H satisfies the condition $H^{\rm P}_{\rm c2} < H \ll H^{\rm orb}_{\rm c2}$ at low temperature, with the conventional Pauli-limiting field $H^{\rm P}_{\rm c2} = \sqrt{2}\Delta_0/g\mu_{\rm B}$ and the electronic g factor g. Thus, the density of vortices is not large, and each vortex is sufficiently separated from other vortices. In this situation, we may consider that the PDW state is stabilized also in the vortex lattice state. Indeed, focusing on a single vortex, which is far separated from the other vortices, we have already showed that a self-consistent solution of the order parameter exists only in the PDW state in high magnetic fields $\mu_{\rm B}H/T_{\rm c0} \gtrsim 1.5$ [27]. In such a high magnetic field, the vortex solution of the order parameter in the BCS state does not exist since the BCS state is completely suppressed by the paramagnetic depairing effect [27]. This is consistent with the result in the paramagnetic limit [11].

In the short-coherence-length situation discussed above, the dominant paramagnetic depairing effect stabilizes the PDW state in the vortex state. Hence, we assume SCs with a large Maki parameter $\alpha_{\rm M} = \sqrt{2}H^{\rm orb}_{\rm c2}/H^{\rm P}_{\rm c2}$ [33]. This situation is often realized in heavy-fermion compounds. One of the promising candidate compounds in which the paramagnetic depairing effect plays a dominant role in the Cooper pair destruction mechanism is a representative heavy-fermion SC, $CeCoIn_5$ [34]. Thus, it is plausible that the epitaxial heavy-fermion superlattice $CeCoIn_5$/$YbCoIn_5$ is a candidate compound of the PDW state. Indeed, it shows a large value of $H^{\rm orb}_{\rm c2}$ [6,13] (i.e., large $\alpha_{\rm M}$) as in the bulk $CeCoIn_5$.

B. Particle-hole symmetry in mirror subsector

The suppression of the paramagnetic depairing effect in the PDW state is related to particle-hole symmetry in the mirror subsector. A subsector Hamiltonian in the bilayer PDW state is equivalent to the Hamiltonian of two-dimensional Rashba SCs [28], in which the particle-hole symmetry is preserved. In two-dimensional Rashba SCs, the paramagnetic depairing is suppressed in a Zeeman field parallel to the z axis when the SOC is sufficiently large. This is an intuitive understanding of the paramagnetic depairing suppressed in the PDW state.

On the other hand, the BCS state is affected by the paramagnetic depairing effect. The mirror subsector in the BCS state lacks particle-hole symmetry due to the existence of an interlayer coupling and a Zeeman field. Thus, a subsector Hamiltonian is no longer the Hamiltonian of SCs. Then, the BCS state is affected by the paramagnetic depairing effect, and the ZEP splits off.

The order parameter in a layer in both BCS and PDW states can be viewed as a uniform isotropic s-wave pairing without center-of-mass momentum of Cooper pairs. Thus, one can just seek the conventional vortex solution without the Fulde-Ferrell-Larkin-Ovchinnikov (FFLO) modulation within the layer by using self-consistent calculations. The FFLO vortex core does not necessarily possess the zero-energy states, unlike the PDW vortex core. As shown in Refs. [35,36], the zero-energy LDOS at the vortex core splits into two peaks at finite energies due to the Zeeman field, and each peak corresponds to a spin component. It is possible to distinguish the PDW vortex core from the FFLO one by investigating the presence or absence of zero-energy quasiparticle bound states at the vortex center. We again stress that unusual spectral features in the PDW state come from the SOC and particle-hole symmetry of the mirror subsector.

C. Sudden vortex-core shrinkage

As shown in Fig. 7(b), a large bulk spectral gap $\Delta E(k)$ opens at $E_{\rm F}$ in the PDW state, while a small energy gap appears in the BCS state [Fig. 7(a); note that Fig. 7 depicts

the energy spectra for only one subsector Hamiltonian]. This results from the particle-hole symmetry (asymmetry) in the mirror subsector in the PDW (BCS) state. The vortex-core radius is characterized by the coherence length, which is inversely proportional to the magnitude of $\Delta E(k)$. In the BCS state, the small $\Delta E(k)$ gives rise to the large vortex-core size. On the other hand, the large $\Delta E(k)$ appears due to the change in the internal structure of the Cooper pair by increasing the magnetic field through the BCS-PDW transition, leading to a sudden vortex-core shrinkage.

A possible manifestation of the BCS-PDW phase transition may be observed in an entropy jump, giving rise to the increase in superlattice temperature as the latent heat through the BCS-PDW first-order transition [11] with increasing magnetic field. In general, it is difficult to observe bulk quantities in thin films. However, the site-selective NMR experiment has succeeded in $CeCoIn_5/YbCoIn_5$ epitaxial superlattices [37]. Thus, in the vicinity of the BCS-PDW transition field, the zero-energy DOS obtained from the NMR spectra might depend on a magnetic field sublinearly, reflecting the decrease of low-energy excitations due to the vortex-core shrinkage. This change in the low-energy excitations may occur not only in the isotropic s-wave state studied in this paper but also in the d-wave pairing state expected in $CeCoIn_5/YbCoIn_5$ superlattices. Direct observation of the vortex-core shrinkage by STM/STS is also a promising way to detect the BCS-PDW transition.

VII. SUMMARY

We have numerically investigated the electronic structure of a vortex core in bilayer Rashba SCs by means of the self-consistent quasiclassical calculation. We found that the LDOS structure in the PDW state is quite different from that in the BCS state. The zero-energy vortex bound state exists in the PDW state, whereas it is absent in the BCS state due to the Zeeman effect. This prominent difference stems from (i) the presence or absence of particle-hole symmetry in the mirror subsector of the block-diagonalized BdG Hamiltonian and (ii) the internal structure of the Cooper pair influenced by the SOC. Another intriguing feature of the PDW state is the small vortex-core size compared with the BCS state, leading to a sudden shrinkage of vortex cores through the BCS-PDW phase transition. The characteristic vortex-core structure in the PDW state may be observed by STM/STS and/or NMR measurements at low temperatures. The exotic superconducting phase under a magnetic field may be identified by investigating these features.

ACKNOWLEDGMENTS

We thank M. Kato for fruitful discussions and reading the manuscript. We also thank T. Kawakami, N. Kurosawa, T. Park, and Y. Matsuda for helpful discussions and comments. The computation in this work was done using the facilities of the Supercomputer Center of the Institute for Solid State Physics, The University of Tokyo. T.Y. is supported by a JSPS Fellowship for Young Scientists. This work was supported by the "Topological Quantum Phenomena" (Grant No. 25103711) and "J-Physics" (Grant No. 15H05884) Grant-in Aid for Scientific Research on Innovative Areas from MEXT of Japan and by JSPS KAKENHI Grants No. 24740230, No. 15K05164, and No. 15H05745.

[1] M. Sigrist and K. Ueda, Phenomenological theory of unconventional superconductivity, Rev. Mod. Phys. **63**, 239 (1991).

[2] Y. Maeno, S. Kittaka, T. Nomura, S. Yonezawa, and K. Ishida, Evaluation of Spin-Triplet Superconductivity in Sr_2RuO_4, J. Phys. Soc. Jpn. **81**, 011009 (2012).

[3] *Non-centrosymmetric Superconductors*, edited by E. Bauer and M. Sigrist, Lecture Notes in Physics Vol. 847 (Springer, Berlin, 2012).

[4] T. Yoshida, D. Maruyama, and Y. Yanase, Exotic superconductivity induced by local inversion symmetry breaking, Solid State Phys. **49**, 109 (2014) (in Japanese).

[5] M. Sigrist, D. F. Agterberg, M. H. Fischer, J. Goryo, F. Loder, S.-H. Rhim, D. Maruyama, Y. Yanase, T. Yoshida, and S. J. Youn, Superconductors with Staggered Non-centrosymmetricity, J. Phys. Soc. Jpn. **83**, 061014 (2014).

[6] Y. Mizukami, H. Shishido, T. Shibauchi, M. Shimozawa, S. Yasumoto, D. Watanabe, M. Yamashita, H. Ikeda, T. Terashima, H. Kontani, and Y. Matsuda, Extremely strong-coupling superconductivity in artificial two-dimensional Kondo lattices, Nat. Phys. **7**, 849 (2011).

[7] Y. Nishikubo, K. Kudo, and M. Nohara, Superconductivity in the Honeycomb-Lattice Pnictide SrPtAs, J. Phys. Soc. Jpn. **80**, 055002 (2011).

[8] D. Xiao, G.-B. Liu, W. Feng, X. Xu, and W. Yao, Coupled Spin and Valley Physics in Monolayers of MoS_2 and Other Group-VI Dichalcogenides, Phys. Rev. Lett. **108**, 196802 (2012).

[9] M. H. Fischer, F. Loder, and M. Sigrist, Superconductivity and local noncentrosymmetricity in crystal lattices, Phys. Rev. B **84**, 184533 (2011).

[10] D. Maruyama, M. Sigrist, and Y. Yanase, Locally Noncentrosymmetric Superconductivity in Multilayer Systems, J. Phys. Soc. Jpn. **81**, 034702 (2012).

[11] T. Yoshida, M. Sigrist, and Y. Yanase, Pair-density wave states through spin-orbit coupling in multilayer superconductors, Phys. Rev. B **86**, 134514 (2012).

[12] T. Yoshida, M. Sigrist, and Y. Yanase, Complex-Stripe Phases Induced by Staggered Rashba Spin-Orbit Coupling, J. Phys. Soc. Jpn. **82**, 074714 (2013).

[13] S. K. Goh, Y. Mizukami, H. Shishido, D. Watanabe, S. Yasumoto, M. Shimozawa, M. Yamashita, T. Terashima, Y. Yanase, T. Shibauchi, A. I. Buzdin, and Y. Matsuda, Anomalous Upper Critical Field in $CeCoIn_5/YbCoIn_5$ Superlattices with a Rashba-Type Heavy Fermion Interface, Phys. Rev. Lett. **109**, 157006 (2012).

[14] C. Dubois, G. Santi, I. Cuttat, C. Berthod, N. Jenkins, A. P. Petrović, A. A. Manuel, O. Fischer, S. M. Kazakov, Z. Bukowski, and J. Karpinski, Scanning Tunneling

Spectroscopy in the Superconducting State and Vortex Cores of the β-Pyrochlore KOs_2O_6, Phys. Rev. Lett. **101**, 057004 (2008).

[15] Z. Sun, M. Enayat, A. Maldonado, C. Lithgow, E. Yelland, D. C. Peets, A. Yaresko, A. P. Schnyder, and P. Wahl, Dirac Surface States and Nature of Superconductivity in Noncentrosymmetric BiPd, Nat. Commun. **6**, 6633 (2015).

[16] N. Hayashi, Y. Kato, P. A. Frigeri, K. Wakabayashi, and M. Sigrist, Basic properties of a vortex in a noncentrosymmetric superconductor, Phys. C (Amsterdam, Neth.) **437**, 96 (2006).

[17] J.-P. Xu, C. Liu, M.-X. Wang, J. Ge, Z.-L. Liu, X. Yang, Y. Chen, Y. Liu, Z.-A. Xu, C.-L. Gao, D. Qian, F.-C. Zhang, and J.-F. Jia, Artificial Topological Superconductor by the Proximity Effect, Phys. Rev. Lett. **112**, 217001 (2014).

[18] J.-P. Xu, M.-X. Wang, Z. L. Liu, J.-F. Ge, X. Yang, C. Liu, Z. A. Xu, D. Guan, C. L. Gao, D. Qian, Y. Liu, Q.-H. Wang, F.-C. Zhang, Q.-K. Xue, and J.-F. Jia, Experimental Detection of a Majorana Mode in the core of a Magnetic Vortex inside a Topological Insulator-Superconductor $Bi_2Te_3/NbSe_2$ Heterostructure, Phys. Rev. Lett. **114**, 017001 (2015).

[19] D. J. Yu, F. Yang, L. Miao, C. Q. Han, M.-Y. Yao, F. Zhu, Y. R. Song, K. F. Zhang, J. F. Ge, X. Yao, Z. Q. Zou, Z. J. Li, B. F. Gao, C. Liu, D. D. Guan, C. L. Gao, D. Qian, and J.-f. Jia, Fully gapped s-wave-like superconducting state and electronic structure in $Ir_{0.95}Pd_{0.05}Te_2$ single crystals with strong spin-orbital coupling, Phys. Rev. B **89**, 100501 (2014).

[20] Y. Nagai and H. Nakamura, Multi-band Eilenberger theory of superconductivity: Systematic low-energy projection, arXiv:1507.06039.

[21] N. Hayashi, K. Wakabayashi, P. A. Frigeri, and M. Sigrist, Temperature dependence of the superfluid density in a noncentrosymmetric superconductor, Phys. Rev. B **73**, 024504 (2006).

[22] Y. Higashi, Y. Nagai, and N. Hayashi, Impurity Effect on the Local Density of States around a Vortex in Noncentrosymmetric Superconductors, JPS Conf. Proc. **3**, 015003 (2014).

[23] P. A. Frigeri, D. F. Agterberg, I. Milat, and M. Sigrist, Phenomenological theory of the s-wave state in superconductors without an inversion center, Eur. Phys. J. B **54**, 435 (2006).

[24] L. Kramer and W. Pesch, Core Structure and Low-Energy Spectrum of Isolated Vortex Lines in Clean Superconductors at $T \ll T_c$, Z. Phys. **269**, 59 (1974).

[25] J. E. Sonier, J. H. Brewer, and R. F. Kiefl, μSR studies of the vortex state in type-II superconductors, Rev. Mod. Phys. **72**, 769 (2000).

[26] N. Hayashi, Y. Kato, and M. Sigrist, Impurity effect on Kramer-Pesch core shrinkage in s-wave vortex and chiral p-wave vortex, J. Low Temp. Phys. **139**, 79 (2005).

[27] Y. Higashi, Y. Nagai, T. Yoshida, and Y. Yanase, Vortex Core Structure in Multilayered Rashba Superconductors, J. Phys. Conf. Ser. **568**, 022018 (2014).

[28] T. Yoshida, M. Sigrist, and Y. Yanase, Topological Crystalline Superconductivity in Locally Noncentrosymmetric Multilayer Superconductors, Phys. Rev. Lett. **115**, 027001 (2015).

[29] Y. Ueno, A. Yamakage, Y. Tanaka, and M. Sato, Symmetry-Protected Majorana Fermions in Topological Crystalline Superconductors: Theory and Application to Sr_2RuO_4, Phys. Rev. Lett. **111**, 087002 (2013).

[30] J. Alicea, Majorana fermions in a tunable semiconductor device, Phys. Rev. B **81**, 125318 (2010).

[31] A. Shitade and Y. Nagai, Orbital angular momentum in a nonchiral topological superconductor, Phys. Rev. B **92**, 024502 (2015).

[32] Y. Masaki and Y. Kato, Impurity Effects on Bound States in Vortex Core of Topological s-Wave Superconductor, J. Phys. Soc. Jpn. **84**, 094701 (2015).

[33] Y. Matsuda and H. Shimahara, Fulde-Ferrell-Larkin-Ovchinnikov State in Heavy Fermion Superconductors, J. Phys. Soc. Jpn. **76**, 051005 (2007).

[34] J. D. Thompson and Z. Fisk, Progress in Heavy-Fermion Superconductivity: Ce115 and Related Materials, J. Phys. Soc. Jpn. **81**, 011002 (2012).

[35] T. Mizushima, K. Machida, and M. Ichioka, Topological Structure of a Vortex in the Fulde-Ferrell-Larkin-Ovchinnikov State, Phys. Rev. Lett. **95**, 117003 (2005).

[36] M. Ichioka, H. Adachi, T. Mizushima, and K. Machida, Vortex state in a Fulde-Ferrell-Larkin-Ovchinnikov superconductor based on quasiclassical theory, Phys. Rev. B **76**, 014503 (2007).

[37] T. Yamanaka, M. Shimozawa, R. Endo, Y. Mizukami, H. Shishido, T. Terashima, T. Shibauchi, Y. Matsuda, and K. Ishida, Interface between heavy fermions and normal electrons investigated by spatially resolved nuclear magnetic resonance, Phys. Rev. B **92**, 241105(R) (2015).